JOURNAL OF THE MECHANICAL BEHAVIOR OF BIOMEDICAL MATERIALS 20 (2013) 387–397

Available online at www.sciencedirect.com

SciVerse ScienceDirect

www.elsevier.com/locate/jmbbm

Research Paper

Multiscale design of surface morphological gradient for osseointegration

Junning Chen[a], *Chaiy Rungsiyakull*[a,b], *Wei Li*[a], *Yuhang Chen*[a,c], *Michael Swain*[d], *Qing Li*[a,*]

[a]*School of Aerospace, Mechanical and Mechatronic Engineering, The University of Sydney, NSW 2006, Australia*
[b]*Department of Mechanical Engineering, Chiang Mai University, Muang 50200, Thailand*
[c]*School of Engineering and Physical Sciences, Heriot-Watt University, Edinburgh EH14 4AS, UK*
[d]*Faculty of Dentistry, The University of Sydney, NSW 2006, Australia*

ARTICLE INFO

Article history:
Received 31 May 2012
Received in revised form
21 August 2012
Accepted 24 August 2012
Available online 1 September 2012

Keywords:
Osseointegration
Porous implant
Topography optimization
Multiscale modeling
Bone remodeling
Material design optimization
Finite element

ABSTRACT

Rapid and stable osseointegration signifies a major concern in design of implantable prostheses, which stimulates continuous development of new implant materials and structures. This study aims to develop a graded configuration of a bead/particle coated porous surface for implants by exploring how its micromechanical features determine osseointegration through multiscale modeling and remodeling techniques. A typical dental implantation setting was exemplified for investigation by using the remodeling parameters determined from a systematic review of bone-implant-contact (BIC) ratio published in literature. The global responses of a macroscale model were obtained through 48 month remodeling simulation, which forms the basis for the 27 microscopic models created with different particle gradients ranging from 30 to 70 μm. The osseointegration responses are evaluated in terms of the BIC ratio and the averaged 10% peak Tresca shear stress (PTS). Within the sampling designs considered, the configuration with 50-30-30 μm particle sizes provides the best outcome, counting 20% more BIC ratio and 0.17 MPa less PTS compared with the worst case scenario, also outperforming the best uniform morphology of 70 μm particles. Furthermore, the response surface method (RSM) was utilized to formulate the bone remodeling responses in terms of gradient parameters across three layers. Gradient 30.0-30.0-32.1 is found an optimal gradient for BIC ratio, and 70-45.4-40.8 the best for the minimum PTS. The multiobjective optimization was finally performed to simultaneously maximize BIC ratio and minimize PTS for achieving the best possible overall outcome. Due to strong competition between these two design objectives, a Pareto front is generated. To make a proper trade-off, the minimum distance selection criterion is considered and the gradient of 37.1-70.0-67.7 appears an optimal solution. This study provides a novel surface configuration and design methodology for individual patient that allow optimizing topographical gradient for a desirable patient-specific biomechanical environment to promote osseointegration.

*Corresponding author. Tel.: +61 2 9351 8607; fax: +61 2 9351 7060.
E-mail address: Qing.Li@sydney.edu.au (Q. Li).

1751-6161/$ - see front matter © 2012 Elsevier Ltd. All rights reserved.
http://dx.doi.org/10.1016/j.jmbbm.2012.08.019

1. Introduction

Over the last two decades, titanium endosseous implants have been well accepted as effective management tool for restoring oral functions in the orofacial structures (Dewidar and Lim, 2008; Morra et al., 2003). Titanium and its alloys are of proven mechanical properties and biocompatibility favored by osseointegration that is the key for implant to anchor onto the host bone (Kunzler et al., 2007; Morra et al., 2003; Rungsiyakull et al., 2010; Li et al., 2011). Nevertheless, there are still some biomechanical drawbacks for titanium implants, such as limited or delayed bone growth into or around the implant surface (Rungsiyakull et al., 2010; Vaillancourt et al., 1995). In order to enhance osseointegration, various physical and chemical surface treatment technologies have been developed to achieve desirable surface morphologies (Esposito et al., 1998; Kunzler et al., 2007; Rungsiyakull et al., 2010). A porous implant surface provides considerably more space to promote cell attachment and tissue ingrowth, thereby facilitating a higher level of bone-implant interaction for cell migration and osteoblast adhesion to the implant surfaces (Anil et al., 2011; Esposito et al., 1998; Morra et al., 2003; Okazaki et al., 1991; Xue et al., 2007). As a result, a more even shear stress can be transferred across the interface, leading to a more uniform stimulation to the surrounding tissues for the establishment of osseointegration and biomechanical binding. The performance of porous surface relies on a number of topographical features, including porosity, pore/particle size, pore orientation, etc.

Various in vivo empirical studies have been carried out to determine the effects of these factors (Itala et al., 2001; Morra et al., 2003; Suzuki et al., 1997; Vaillancourt et al., 1995). In general, increasing porosity to a certain extent can provide a greater space to enable more efficient nutrient delivery and metabolite removal for cellular activities, thereby better promoting bone mineralization and stabilization over a shorter period (Morra et al., 2003; Vaillancourt et al., 1995). Shen et al. (2008) developed computational models to determine the effects of porosity and particle sizes of porous titanium and their further study modeled the bone's responses to surface morphology (Shen and Brinson, 2011). Rungsiyakull et al., (2010) found the combinations of particle sizes and porosities at 100 μm, 65% and 38 μm, 82.5% could be favored for cortical and cancellous bone remodeling under the uniform surface morphology settings, respectively.

Nevertheless, these existing studies have considered nearly uniform morphology across the porous thickness, in which there is no systematic variation in pore or particle size and porosity except for microscopic randomness. On the other hand, there is a new opportunity to improve bone osseointegration and remodeling by adopting graded surface morphology that has been proposed as a potential upgrade to existing uniform coated implants (Kim et al., 2010; Yang and Xiang, 2007; Yang et al., 2002, 2000). Over the past decade, material scientists and engineers have been attempting to develop different morphological gradients to lower the mismatching of mechanical properties and improve osseointegration between bone and implant (Kunzler et al., 2007; Yang and Xiang, 2007). A few empirical studies have been carried out to evaluate biocompatibilities and advantages of graded surfaces in promoting bone ingrowth (Chen et al., 2006; Kunzler et al., 2007; Yang et al., 2002, 2000). Computational models of axially graded hydroxyapatite-titanium solid implants were proposed by Lin et al., (2010b) for a macroscopic level of material design, and some rather indicative results were generated to seek optimal gradient for osseointegration (Yang and Xiang, 2007; Lin et al., 2009b). However, all these studies focused on macroscopic responses and considered only the axial gradients with solid composites. Very few reports have been available to model a graded porous surface morphology in radial direction through examining microscopic responses and none has genuinely searched for an optimal radial gradient to date.

This paper aims to provide a multiscale study for bone remodeling responses and provide a new approach to examining the effects of different combinations of particles/beads for a graded surface morphology, with sizes varying from 30 to 70 μm. As one of the most critical indicators to implant success, osseointegration is measured in terms of ongoing bone-implant contact (BIC) ratio and an average of top 10% Tresca shear stress (PTS) in the peri-implant regions. Based on the remodeling results obtained, the response surface method is adopted to formulate the osseointegration outcomes in terms of gradient parameters, thereby determining an optimal gradient configuration for particle coating.

2. Material & methods

2.1. *Multiscale finite element (FE) modeling*

With rapid development of fabrication technologies for micro- and/or nanostructured materials, traditional monoscale finite element analysis (FEA) became inadequate to capture detailed interaction between biomaterials and tissues effectively. In order to tackle this problem, multiscale analysis techniques have been developed by bridging macroscale (global) homogenized materials to microscale (local) heterogeneous structures, enabling more insightful analysis (Podshivalov et al., 2011a, 2011b; Rungsiyakull et al. 2010). Multiscale modeling has been used to simulate how bone is related to internal structures and implant compositions (Fritsch et al., 2009), how trabecular bone remodels for correlating to empirical data (Buti et al., 2010), and how surface morphology affects local cancellous and cortical osseointegration (Rungsiyakull et al., 2010).

This paper concerns a non-threaded implant to better restrict our attention on the specific effect of surface morphology gradient rather than other geometric features on osseointegration. To avoid the structural complexity of the 3D multiscale model and associative high computational costs for remodeling analyses (Romeed et al., 2006), a 2D model capable of capturing the major biomechanical features in the occlusal loading scenario of mandible section is adopted in this study (Rungsiyakull et al., 2010). As a preliminary study on topographical gradients, the 2D model facilitates capturing many randomly-located particles/beads and pores in a reasonably dense mesh, requiring relatively lower computational cost for iterative remodeling simulations

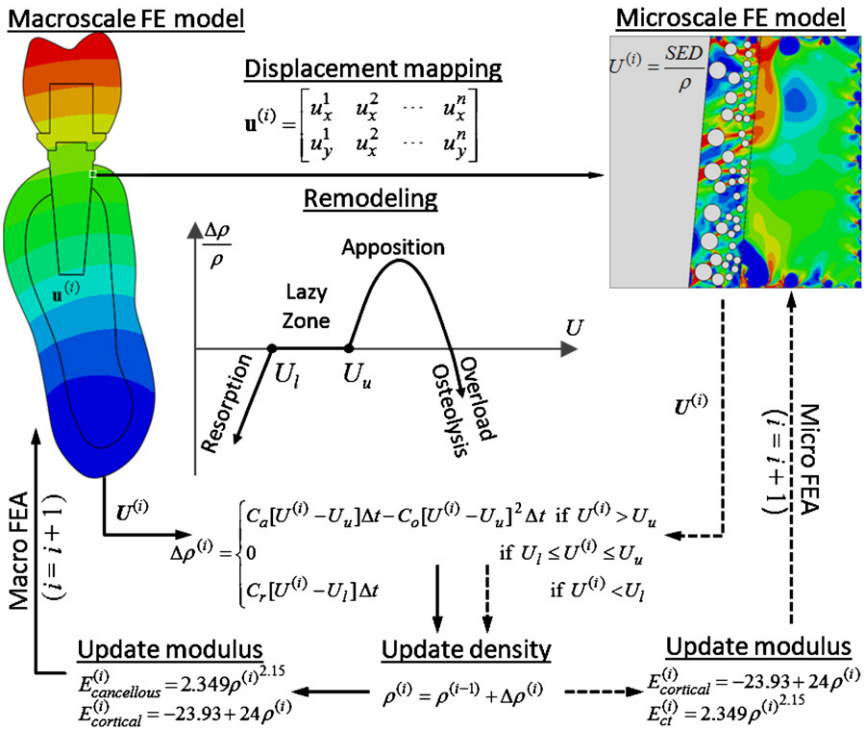

Fig. 1 – Remodeling algorithm with the adjusted Wolff's Law as the major governing equation.

compared to the 3D version of multiscale models. Other computational pros and cons between 2D and 3D models can be consulted from literature (Romeed et al., 2006).

The implant considered herein is coated through sintering beads and has a 5 degree taper angle (Vaillancourt et al., 1995) (Fig. 1). This global model comprised an abutment and a ceramic crown as typical dental implantation setting. A 202.23 N load was applied vertically to the crown cusp with 2 mm horizontal offset from the center to the buccal side (Lin et al., 2010b; Rungsiyakull et al., 2010). Note that the details of microscopic morphology were not considered in the global model.

Microscale models were created by selecting a representative region of 1 mm × 1 mm in the cortical region, consisting of bone, implant, and a 300 μm transitional region between them, which presents a mixture of pores due to the bead morphology and connective tissues growing from host bone (Rungsiyakull et al., 2010). To explore the effect of the coating gradient on osseointegration, this transitional area was separated into three layers with different combinations of particle sizes (specifically, 30, 50, and 70 μm in diameter (Bobyn et al., 1980; Rungsiyakull et al., 2010)) to form a graded surface morphology. Each layer has 3 candidate particle sizes, leading to $3 \times 3 \times 3 = 27$ different surface morphologies, including 24 graded and 3 uniform configurations. Note that current fabrication technologies have been capable of providing various porosities across a range from 30% to 70%, with which these implants can still have adequate mechanical properties for loading-bearing and other biomechanical requirements (Dewidar and Lim, 2008; Traini et al., 2008; Xue et al., 2007). Thereby, the volume fraction (counted as area fraction in 2D) of implant beads was kept constant at 30% (highest available porosity) to focus more on the effects due to particle sizes and morphological gradient. Thus, 27 microscopic sample models were created to represent all possible gradients determined by the given design parameters. Linear triangular element was chosen to mesh macroscale and microscale models after a convergence test by using total strain energy (Li et al., 2005).

2.2. *Material properties*

In the macroscale model, the implant core adopted the properties of commercial titanium alloy, Ti6A14V (O'Brien, 2008), and the abutment and crown are zirconia (Lin et al., 2010b). The initial properties of the cortical and cancellous bones follow the empirical data (Carr and Carr, 1995; O'Brien, 2008). Here comes the first assumption that the Poisson's ratio of the same type of tissue does not vary with changing Young's modulus to simplify the analysis. Similarly in the micro models, the implant region and the cortical bone region adopt the same properties as those in the macro models, and the second assumption is that the transitional region is fully filled by blood clot after 30 min of implantation (Riha et al., 1999) as its initial status. All the material properties used in this simulation are summarized in Table 1, and were assumed to be linearly elastic and isotropic to simplify the remodeling analysis (Rungsiyakull et al., 2010). The minimum Young's modulus was set as 870 MPa and minimum density as 0.85 g/cm^3 to allow remodeling to low density tissues (Rungsiyakull et al., 2010). Following the previous studies, the average density of cortical bone is allowed to approach its upper limit of 2.0 g/cm^3 (Lin et al., 2009a; 2010a; Rungsiyakull et al., 2010).

Table 1 – Initial properties of multiscale models for remodeling simulation.

	Macroscale model			
	Implant core	Abutment & crown	Cortical bone	Cancellous bone
Young's Modulus (MPa)	110,000 (Chen et al., 2011)	201,000 (O'Brien, 2008)	1970 (Lin et al., 2010)	14.8 (Carr and Carr, 1995)
Poisson Ratio	0.35 (O'Brien, 2008)	0.28 (O'Brien, 2008)	0.33 (Lin et al., 2010)	0.33 (Carr and Carr, 1995)

	Microscale model					
	Native bone (cortical)	Implant core & beads	Hosting tissue (blood clots)	Mature bone	Immature bone	Soft tissues
Young's Modulus (MPa)	1970 (O'Brien, 2008)	110,000 (Carr and Carr, 1995)	0.001 (O'Brien, 2008)	6000 (Riha et al., 1999)	1000 (Liu and Niebur, 2008)	1 (Liu and Niebur, 2008)
Poisson Ratio	0.33 (Liu and Niebur, 2008)	0.3 (Carr and Carr, 1995)	0.33 (O'Brien, 2008)	0.33 (Carr and Carr, 1995)	0.33 (Carr and Carr, 1995)	0.167 (Carr and Carr, 1995)

2.3. *Multiscale remodeling*

The Wolff's rule forms the major governing equations for modeling the turnovers of cortical, cancellous bone, and connective tissues (Frost, 2003; Keaveny, 2001; Lin et al., 2009a; Rungsiyakull et al., 2010). In this simulation, the time increment was set to be a month, and the mechanical stimuli is the difference between an instant strain energy density (SED) per unit mass ($U^{(i)} = \sigma\varepsilon/2\rho$) and either upper or lower reference SED per unit mass (U_l, U_u), which are 10% offset from their mean (Keaveny, 2001; Lin et al., 2010a, 2009b). The rates of bone apposition and resorption were presented by C_a and C_r, respectively (Lin et al., 2010a, 2009b). Mechanical overload is also taken into account in this study, which can induce bone loss by presenting osteolysis if it exceeds the physiological limit (Esposito et al., 1998; Noble and Reeve, 2000; Wernig and Xu, 2000; Xie et al., 2010). A quadratic term is added to the remodeling equation for such an adjusted Wolff's rule (see Fig. 1) (Field et al., 2010; Field et al., 2012; Lin et al., 2009a; Li et al., 2007; Tanaka et al., 1999; Field et al., 2010; 2012).

The upper and lower reference SED per unit mass were set at 0.000021 and 0.000033 J cm^3/g, respectively (Rungsiyakull et al., 2010). The remodeling rate coefficients, C_a, C_o, and C_r (see Fig. 1), were determined by matching the simulation results to the in-vivo data in terms of bone-implant-contact (BIC) ratios from literature. The new bone density determined by the Wolff's rule updated Young's modulus of bony tissues. In this study, the connective tissue will follow the cancellous remodeling equation because its Young's modulus is much lower than the threshold of cortical bone (6 GPa). Displacement fields generated in the macroscale remodeling is mapped to the microscale models as the inputs. Both macroscale and microscale remodeling procedures were implemented in FORTRAN code through the ABAQUS user subroutine.

2.4. *Design optimization*

First, the bone-implant-contact (BIC) ratio is considered one of the primary measures to osseointegration, which measures the degree how the bone ingrows into and becomes mature in the pore space of the transitional region (Liu and Niebur, 2008; Sollazzo et al., 2008). The BIC ratio can be determined by the proportion of elemental areas with Young's modulus higher than the threshold of mature bone (MB) to the total element volume (or area in 2D models as in this paper) of connecting tissues as follows:

$$f_{BIC} = \%BIC = \frac{Mature\ Bone\ Area}{Total\ Elemental\ Areas} \times 100\% = \frac{\sum_{j=1}^{MB} A_j}{\sum_{i=1}^{AE} A_i} \times 100\% \quad (1)$$

The other concern lies in whether implant-bone interface can withstand mechanical loading without debonding failure. Indeed, the pull-out test has been an important method to test the extent of osseointegration in terms of shear resistance (Abron et al., 2001; Anderson et al., 1984; Bobyn et al., 1980; Feighan et al., 1995). For this reason, Tresca stress is adopted as another key measure to implant topography, assessing how well the surface morphological gradient alleviates the shear stress concentration. Note that the maximum Tresca stress in a single element may not be appropriate to determine the shear failure for entire region, and to make it more statistically meaningful, the elemental Tresca stresses averaged out over 10% of the total volume (area in 2D models) with the highest stress concentration is adopted. Therefore the overall risk of shear failure is measured as

$$f_{PTS} = \frac{\sum_{e=1}^{n} Peak\ Tresca\ Stress\ (Top\ 10\%) \times Elemental\ Area}{Total\ Elemental\ Area\ of\ Top\ 10\%\ Tresca\ Stress} = \frac{\sum_{e=1}^{n} \sigma_{Tre}^{e} \times A_{Tre}^{e}}{\sum_{e=1}^{n} A_{Tre}^{e}} \quad (2)$$

where n is the number of elements giving a sum of 10% the total area.

To seek an optimal design, the particle sizes in the three layers, α_1, α_2, and α_3, will be varied to see if an optimal outcome of osseointegration can be attained. To do so we introduce multiobjective optimization technique to maximize BIC and minimize PTS by using linearly weighted average (LWA) and multiple objective particle swarm optimization (MOPSO) approaches, respectively.

The LWA method (Hou et al., 2008; Lin et al., 2009b; Rungsiyakull et al., 2010) formulates a cost function by comprising the individual objectives in terms of the selected

weighting factors ω_1 and ω_2 as

$$\begin{cases} \min F_{LWA}(\alpha_1,\alpha_2,\alpha_3) = \omega_1 \dfrac{f^0_{BIC}}{f_{BIC}} + \omega_2 \dfrac{f_{PTS}}{f^0_{PTS}} \\ \text{s.t. } \omega_1 + \omega_2 = 1,\ (\omega_1 \geq 0,\ \omega_2 \geq 0) \\ 30\ \mu m \leq \alpha_1,\alpha_2,\alpha_3 \leq 70\ \mu m \end{cases} \quad (3)$$

To eliminate the dimensional difference in combining these two individual objective functions, the normalization was applied by using minimum f^0_{BIC} and maximum f^0_{PTS} in the design domain.

The particle swarm optimization (PSO) (Raquel and Naval, 2005) method incorporates the mechanism of crowding distance, which is specifically benefited on global best selection of dominated solutions from an external archive. This method allows a fast convergence, and has been successfully applied in a broad range of problems (Hou et al., 2008; Padhye et al., 2009; Raquel and Naval, 2005; Rungsiyakull et al., 2010).

$$\begin{cases} \min F_{MOPSO}(\alpha_1,\alpha_2,\alpha_3) = [f^{-1}_{BIC},\ f_{PTS}]^T \\ \text{s.t. } 30\ \mu m \leq \alpha_1,\alpha_2,\alpha_3 \leq 70\ \mu m \end{cases} \quad (4)$$

2.5. *Response Surface Method (RSM)*

It is by no means easy to establish the objective functions mentioned above. Such surrogate modeling techniques as RSM is considered an effective, and sometimes unique, alternative (Hou et al., 2008; Lin et al., 2009b; Rungsiyakull et al., 2010). Since the knowledge of the objective functions is rather limited; we attempted several different polynomial models to capture sophisticated mutual effects from multiple variables (Bradley, 2007). As such, the most suitable response surface (RS) function was finally determined.

3. Results

In this study, bone remodeling response was simulated by using different surface morphological gradients over the 48 months of healing, in which the host bone can ingrow into the void space and the corresponding osseointegration performance is measured by the BIC ratios and averaged peak Tresca stress (10% volume), respectively. After a certain period of initial healing, bone could gradually achieve a dynamic equilibrium with both apposition and resorption occurring to a similar extent, in which the design parameters are considered less significant. The results in Month 6 and Month 48 were chosen as two critical indications to measure short-term and long-term performances, respectively.

3.1. *Bone-implant-contact (BIC) ratio*

The porosities of each layer in the graded surfaces were kept constant at 70% in this study. In other words, all the models in different layers had the same void space to allow tissue ingrowth. The BIC ratios are presented in a unit of %. All gradient configurations are presented in a form of (α_1–α_2–α_3), representing the particle sizes in different layers in which α_1 is the layer closet to the implant core and α_3 is next to the host bone.

Fig. 2(a) compares the two gradients having the highest and the lowest BIC ratios to the three uniform surface morphologies consisting of 30, 50 and 70 μm particles, and obviously they demonstrate the evident effect of gradients on osseointegration rate. Gradient 50-30-30 shows superior bone mass gain over the entire simulation period than others, and it has 6.41% more bone-implant contact ratio than configuration 70-70-70 by Month 48, which is the best performer of all three uniform ones. However, it is noted that not all graded surface morphologies increase the extent of osseointegration. Gradient 70-30-50 shows a reverse effect on osseous tissue ingrowth, although its initial gain over the first 8 months is higher than uniform configuration 50-50-50, which has the worst outcome in the uniform morphologies.

As shown in Fig. 2(a), all five surface morphologies presented have similar rates of mature bone deposition during the first three months of acute healing. However, there has been a significant difference in BIC outcomes after Month 6. Gradient 50-30-30 maintained a steep growth rate till the end of the first year and started to level off more quickly, while

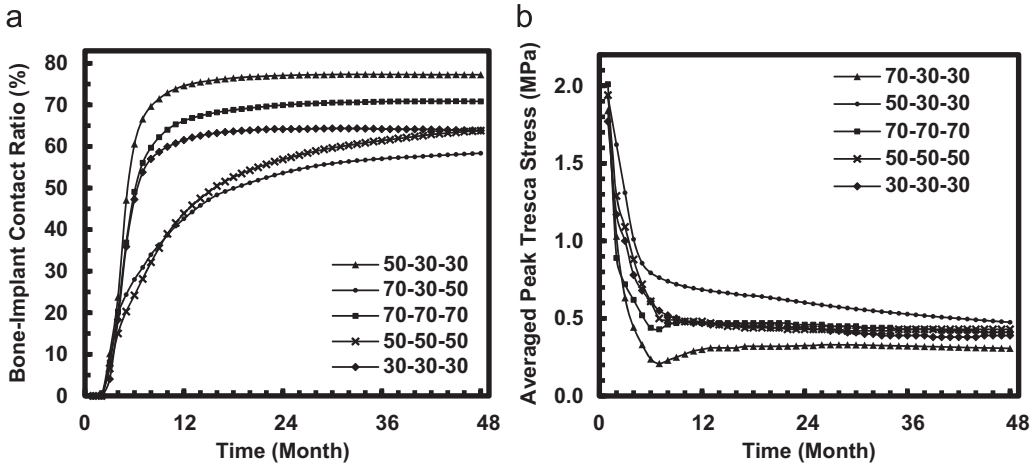

Fig. 2 – Five representative bone-implant contact ratios (a) and highest/lowest average peak Tresca stresses (b) in 27 Samples over 48 month period.

the growth in Gradient 70-30-50, on the other hand, has a delayed take-off and an earlier drop-off, but its growth is more gradual and smoother than Gradient 50-30-30, which lasts for more than 3 years till the mature bone apposition becomes equilibrium. At the end of 48 months, the best and worst gradients ended up with around 20% difference in the BIC ratios.

3.2. *Averaged peak Tresca stress (PTS)*

The averaged PTS (10% of the total volume) is adopted as the other important indicator to measure the success of implantation in this study. Fig. 2(b) plots the overall highest and lowest Tresca stress evolutions of all the 27 gradients compared to those induced by the three uniform morphologies. It is reasonable to see Gradient 70-30-30 delivers the lowest stress concentration over the 48 months. Note that the highest shear failure possibility appears to be in Gradient 50-30-30.

Along the overall trend, the quick drops of PTS in the first 6 months indicate the rapid growth of osseous tissues, and the reductions are 86.9% for Gradient 70-30-30 and 58.5% for Gradient 50-30-30. After that, these two gradients gradually converge towards Month 48. A similar pattern occurs in the uniform surface morphologies which fall between the best and worst. The final difference between Gradients 70-30-30 and 50-30-30 at Month 48 is 0.17 MPa, approximately 10% of the initial stress concentration.

Different to the BIC outcomes, all gradients show a slower and more gradual convergence for PTS. From Fig. 2(b), the PTS bumps back after the quick drop and then levels off to equilibrium over the time, instead of approaching to a steady state straightway as in BIC (Fig. 2(a)). Based on the monthly data obtained, however, it seems unclear to draw a direct relationship between BIC and PTS.

4. Discussion

4.1. *Bone remodeling responses*

Previous in vivo studies have been carried out to explore bone-implant contact problems, and these empirical data can provide an approximate guide to determinate the bone remodeling ratio, by interpreting the solid bone deposition through the object lifespan. Kim et al. (2010) performed an in vivo study on 30 implants in dog mandibles with three groups of different surface finishing. In the roughest surface group, BIC reached 81.2% over 10 weeks. Since the tested subjects were dogs, ten weeks can be interpreted to human life roughly a year and an half in their study. Similarly, Deporter et al. (1990) adopted a porous-coated dental implant showed 50% and 65% BIC in the buccal and lingual sides of dog mandible after 18 weeks of functional loading (or 2.5 year human life). Beside dogs, rabbits are also a popular animal subject. Suzuki et al., (1997) conducted a time-dependent study on rabbit femur by separating them into smooth and rough surface groups. BIC in the rough surface group reached 37%, 62%, and 78% in 6, 16, and 42 weeks, corresponding to human life approximately 1, 2.5, and 7 years, respectively. Abron et al., (2001) also performed a study on rat tibiae and indicated an averaged BIC of 54% in 3 weeks, corresponding to 1.5 year human life. Morra et al.'s in vivo study on rabbits' femoral diaphysis presented an averaged BIC of 62.75% in 12 weeks (2 year human life) (Morra et al., 2003). BIC has also been considered in computational remodeling, for example, Lian et al. (2010) tested four different initial BICs (25, 50, 75 and 100%) without surface morphology. After equilibrium, the final outcomes all fell into a range from 58 to 60% BIC.

By summarising all these data points, a graphic plot of BIC ratios from literature against time (Fig. 3) can show a rough progression trend for human osseointegration, in which a logarithm curve is fitted. It is noted that with the same set of correlated bone remodeling parameters, the comparison between individual graded and uniform surface morphologies becomes valid and meaningful. The BIC outcomes for Gradients 50-30-30 and 70-30-50 have shown reasonable consistencies to the literature data; the former (best) exhibits improved performance above the fitting line and the latter (worst) fall below it for most of time as expected.

The bone conditions of individual patients may vary considerably from one to another, and the corresponding remodeling parameters will certainly affect the simulation outcomes. However, the main interests of this paper reside in establishing a new computational procedure and revealing a fact that different surface gradients lead to different osseointegration outcomes under the same bone and remodeling condition. By using the design protocol established here, a private case study can be performed to create a patient-specific surface gradient, meeting individual needs. Meanwhile, this approach can be extended to a 3D model by including a peripheral gradient for an implant with more sophisticated coating variables.

4.2. *Response surface functions*

The sample data provides the essential information to extrapolate design analysis and optimization. Based on the above remodeling results, the assessment criteria, BIC and PTS, are related to the design variables of coating parameters in each

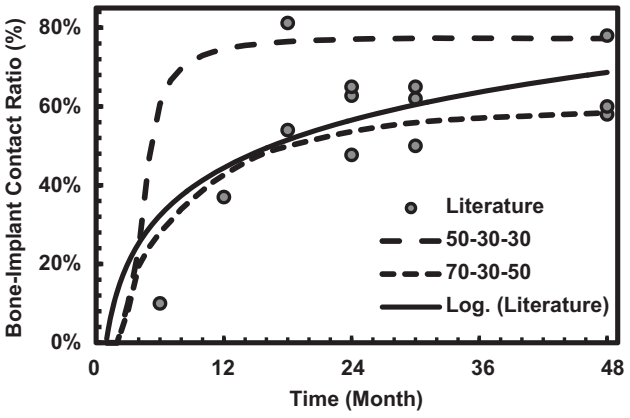

Fig. 3 – Data interpretation and trend line for bone-implant contact ratios from the in vivo animal studies compared to the best (50-30-30) and the worst (70-30-50) remodeling simulation outcomes in the two surface gradients.

Table 2 – Response surface models (Polynomial) for Month 6 and 48.

	Time	RS Model	R-sqr	Max	RSM* Max	Min	RSM* Min	RMSE**
BIC (%)	Month 6	Linear	0.8828	60.59	45.79	21.51	27.33	8.69
		Quadratic	0.9035		50.54		23.02	6.21
		Cubic	0.9536		59.15		21.83	4.30
	Month 48	Linear	0.9950	77.25	71.92	58.36	63.23	4.88
		Quadratic	0.9968		73.69		57.90	3.88
		Cubic	0.9983		76.95		56.66	2.88
PTS (10^5 Pa)	Month 6	Linear	0.9417	9.14	6.50	2.38	4.09	1.35
		Quadratic	0.9572		8.05		3.15	1.16
		Cubic	0.9647		8.89		2.84	1.06
	Month 48	Linear	0.9810	4.96	4.03	2.85	3.64	0.54
		Quadratic	0.9888		4.55		3.21	0.42
		Cubic	0.9942		4.83		3.04	0.31

* Response surface method result.
** Root mean square error.

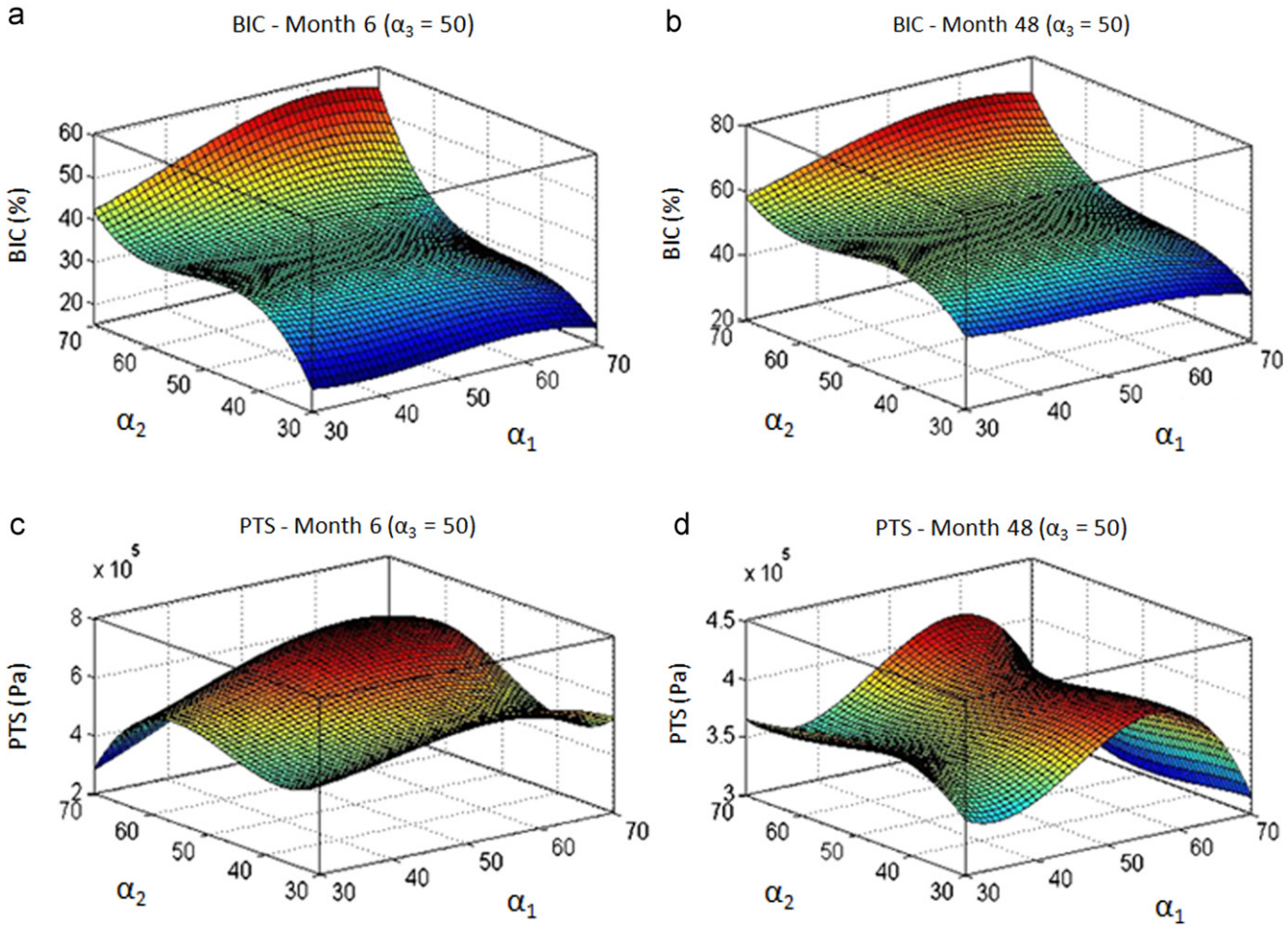

Fig. 4 – Response surfaces showing the effects of gradient input α_1 and α_2 when α_3 is set to 50 μm on BIC and averaged peak Tresca stress at Months 6 and 48, respectively.

layer as (α_1, α_2, α_3,). In order to evaluate the fitness of response surface (RS) models, 3 different orders (linear, quadratic, and cubic) of polynomials were attempted by the least-square method. The R^2 and root mean square error (RMSE) between simulation and RS functions (Max & Min) are used to assess which polynomial is most accurate. As summarized in Table 2, the cubic polynomial functions provide the best fits to both BIC and PTS in these two selected time points for the

short and long term osseointegration (Months 6 and 48, respectively).

To clearly show the response surfaces, α_3 is set to 50 um representing an intermediate size of particles as an example for RSM. Fig. 4a-d plots the BIC and PTS for Months 6 and 48, respectively. From the BIC perspective, the combinations of medium particles in the inner layer (α_1) with large sizes in the mid layer (α_2) shows their advantages over the other configurations in both short term (Month 6 as in Fig. 4a) and long term (Month 48 as in Fig. 4b). Also the trend is affected by α_2 (mid layer) more significantly than α_1 (inner layer), and it drops dramatically along the reverse direction of α_2 axis, with a short level-off at the medium size range. The benefit of using a medium-large combination is being amplified in BIC as healing time progresses. Fig. 4a and b also reflects that Gradient 70-30-50 (right bottom corner in the plots) is the worst performer in the design range over the simulation time.

On the other hand, PTS shows more distinct patterns than BIC. From Fig. 4c, α_2 plays a more important role in the short term osseointegration than α_1; however, this is reversed in the long term as in Fig. 4d. The minimum PTS appears in the case when small particles in the inner layer are combined with the large ones in the mid layer in Month 6, while it occurs at large-medium combinations at month 48. Similarly to BIC, the lowest PTS occurs around Gradient 70-30-50 which is close to Gradient 70-30-30 having the least failure chance.

Based on the RS functions obtained, we can determine the gradients for either maximum BIC or minimum PTS outcomes in both Month 6 and 48, respectively. It is noted that gradient 61.8-70.0-49.9 has the highest BIC ratio as 61.35% in Month 6, but at the same time with a high PTS of 0.54 MPa. In contrast, Gradient 70.0-30.1-70.0 has the lowest PTS of 0.29 MPa accompanied by a lower bone mass gain, leading to a BIC ratio of 29.81%. In Month 48, Gradient 30.0-30.0-32.1 leads to the maximum BIC ratio of 76.92% (0.34 MPa PTS), while Gradient 70-45.4-40.8 provides with the lowest PTS of 0.28 MPa (40.71% BIC). It appears that these two design criteria cannot be achieved concurrently.

4.3. *Multiobjective optimization*

Here we attempt to adopt multiobjective optimization for maximizing BIC and minimizing PTS by using both linearly weighted average (LWA) and direct multiple objective particle swarm optimization (MOPSO) methods.

In the LWA method, one of the weighting factors rises by a small increment of 0.0005 in order to obtain the Pareto frontier, resulting in 80, 000 Pareto points. 80 of them with uniform intervals are selected to plot Pareto fronts in Fig. 5(a) and (b) for Month 6 and Month 48, respectively. The Pareto set is supposed to span the entire optimal solution space. It is observed, however, that highly concentrated regions appear in both Month 6 and Month 48 solutions, with a few isolated aggregates.

To tackle the non-uniform distribution problem occurred in the LWA solutions, the multiobjective Particle Swarm Optimization (MOPSO) method is adopted in line with its special features in generating a well-distributing Pareto solution (Rungsiyakull et al., 2010). 2, 000 Pareto points are generated through 1, 000 iterations, and 80 of them with uniform intervals are plotted in the same graph as that from the LWA method. Obviously, MOPSO is more effective than LWA in terms of the smoothness of Pareto frontier and extent of uniformity in this design problem. As expected, MOPSO is much more widely distributed and all the LWA results are well located in the MOPSO Pareto frontier, which also reflects the effectiveness of these two approaches, although they differ in integrity of outcomes.

From the Pareto frontier generated by MOPSO, the maximum BIC ratio and the minimum PTS cannot be achieved

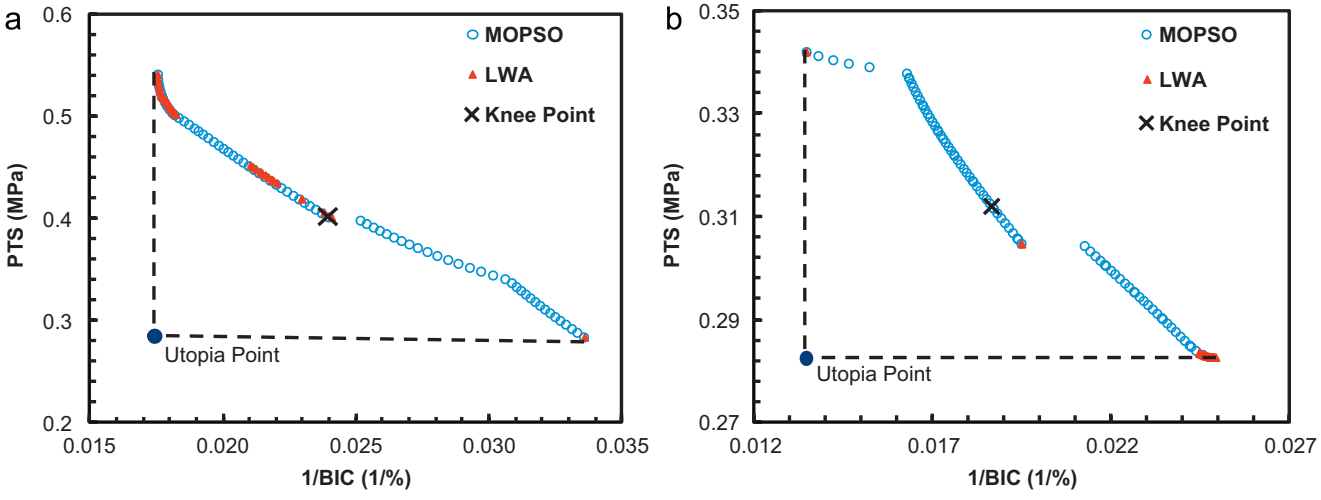

Fig. 5 – Pareto set of optimal surface gradient parameters based on two multiobjective optimization schemes at month 6 and 48, respectively. Any point on the Pareto frontiers represents a feasible solution, and the MOPSO method is more effective than the LWA method to depict the Pareto fronts. Knee point has the shortest distance to the Utopia point which is selected as an optimal solution.

simultaneously. It is noted that further improving either BIC or PTS must sacrifice the corresponding counterpart along the Pareto frontier. For example, acuter and faster bone growth in early stages will be accompanied by a higher peak stress, and vice versa.

There is a Utopia point where the maximum BIC ratio and the minimum PTS occur at the same time; however this point cannot be achieved in most design cases presented (Rungsiyakull et al., 2010). In theory, any point in the Pareto frontier can be a solution to a specific morphological design providing different BIC ratio and PTS, and a full range of optima provides multiple choices on various balances between BIC ratio and PTS for clinical decision. Based on the given selection criteria, a decision can be made for the most "satisfactory" solution, known as a knee point, in the Pareto set (Sun et al., 2011). In this paper, the minimum distance selection method (MDSM) is adopted for an optimal selection, as stated in the following equation:

$$\min D = \sqrt{\left(\frac{f_{BIC}-f^{L}_{BIC}}{f^{U}_{BIC}-f^{L}_{BIC}}\right)^{2}+\left(\frac{f_{PTS}-f^{L}_{PTS}}{f^{U}_{PTS}-f^{L}_{PTS}}\right)^{2}}. \quad (5)$$

In this equation, f_{BIC} and f_{PTS} are the objective functions, while f^{L} and f^{U} are their corresponding upper and lower thresholds in the design space concerned. An optimal gradient can thus be selected by minimizing the distance between the point itself and the Utopia point. Within the limitation of this study, it is found that the coating with a moderate gradient near the largest particle size (70.0-70.0-61.6) represents an optimal solution to initial healing up to Month 6, giving a BIC outcome of 41.53% and PTS of 0.40 MPa. But for the long term healing, a graded coating with a combination of particle size of 37.1-70.0-67.7 is preferred, leading to a BIC ratio of 54.35% and PTS of 0.31 MPa. Note that with other selection criteria, such as "the maximum BIC ratio within a tolerated PTS range", it can lead to a different conclusion on the optimal choice.

4.4. *Patient-specific design and future applications*

Osseointegration process can be affected by both implant surface morphology and physiological conditions. For the latter, age, sex, race, genetics and other biomedical factors all contribute on bone responses to the implantation, leading to different osseointegration outcomes. This paper considers a particular set of remodeling parameters derived from literature to demonstrate how the surface topographical gradient of implant can be optimized for the same given mechanical and biological conditions. With sufficient patient data (e.g. from interval CT/MRI scans), this approach can be used to individual subject with their own remodeling parameters, aiming for a patient-specific design. To each patient, the predicted Pareto optima consist of a series of solutions at different balancing points between BIC ratio and PTS, and a clinic decision can be made based upon individual needs of a patient and clinical expectation.

Although this study takes dental implant as an example, the graded topographical configuration and corresponding design procedure can be extended to other applications of prosthetic fixation, such as orthopedic osseointegration. Recent study has examined the macroscopic remodeling outcomes in terms of bone mass density and failure possibility of different prosthetic designs in hip replacements (Tomaszewski et al., 2012). By applying the design procedure for graded topography proposed in this paper, the microscopic surface morphology can be optimized for the hip prosthesis to meet individual patient needs.

Topology optimization has proven an effective tool for microstructural design aiming to regulate effective material properties for bone remodeling applications (Adachi et al., 2006; Chen et al., 2011, 2009; Sturm et al., 2010). Recent study by Arabnejad Khanoki and Pasini (2012) demonstrated how to optimize microstructural gradient of hip replacement implant for achieving minimum bone resorption and failure probability. Nevertheless, this technique is restricted to periodic microstructures and may be of limited implication to random morphology as shown in this paper.

5. Conclusion

A novel application of multiscale modeling and remodeling analyses has been implemented in this study to optimize a graded porous surface morphology, by evaluating osseointegration outcomes in terms of bone-implant-contact (BIC) and averaged peak Tresca stress (PTS). The simulation results suggested that particles sizes in each surface layer determine bone ingrowth and shear stress distribution, and the optimized surface gradient can outperform the uniform surface morphologies that were adopted in most of traditional implants. A cubic surrogate model is found the best to correlate BIC and PTS to gradient parameters in this problem, and the RS plots fall into a good agreement with the sample simulation results, leading to different gradient optima for the highest BIC ratio or the minimum PTS in Month 6 and 48, respectively. Since the maximization of BIC and minimization of PTS cannot be achieved simultaneously, the multiobjective optimization was adopted here. Two different approaches, namely LWA and MOPSO, were used to generate Pareto solutions, where MOPSO demonstrates its capability of dealing with concentrated regions of optimal solutions. By adopting the minimum distance selection method (TMDSM), Gradients 70.0-70.0-61.6 and 37.1-70.0-67.7 are selected by minimizing the distance to the Utopia point as the most "satisfactory" solutions for short term and long term healing, respectively. With sufficient patient information, a private case study can be conducted by following this procedure to generate a range of optimal solutions, allowing the material engineers to choose patient-specific surface morphology for clinic application. With different optimum selection criteria, a different solution might be obtained. Further animal studies can be performed to verify the multiscale model and graded porous implant surface. The future investigation can also be to optimize porosity gradients under other design criteria (Natali et al., 1997) or with other materials, thereby providing different implant-tissue interaction (e.g. (Chen et al., 2011)).

Acknowledgment

This work was supported by Australian Research Council (ARC) through the Discovery (DP1095140) and Future Fellowship (FT120100947) Schemes.

REFERENCES

Abron, A., Hopfensperger, M., Thompson, J., Cooper, L.F., 2001. Evaluation of a predictive model for implant surface topography effects on early osseointegration in the rat tibia model. The Journal of Prosthetic Dentistry 85 (1), 40–46.

Adachi, T., Osako, Y., Tanaka, M., Hojo, M., Hollister, S.J., 2006. Framework for optimal design of porous scaffold microstructure by computational simulation of bone regeneration. Biomaterials 27 (21), 3964–3972.

Anderson, R.C., Cook, S.D., Weinstein, A.M., Haddad Jr., R.J., 1984. An evaluation of skeletal attachment to LTI pyrolytic carbon, porous titanium, and carbon-coated porous titanium implants. Clinical Orthopaedics and Related Research 182, 242–257.

Anil, S., Anand, P.S., Alghamdi, H., Jansen, J.A., 2011. Dental implant surface enhancement and osseointegration. In: Turkyilmaz, I. (Ed.), Implant Dentistry—A Rapidly Evolving Practice. Rijeka, InTech, pp. 86–90.

Arabnejad Khanoki, S., Pasini, D., 2012. Multiscale design and multiobjective optimization of orthopedic hip implants with functionally graded cellular material. Journal of Biomechanical Engineering 134 (3), 031004.

Bobyn, J.D., Pilliar, R.M., Cameron, H.U., Weatherly, G.C., 1980. The optimum pore size for the fixation of porous-surfaced metal implants by the ingrowth of bone. Clinical Orthopaedics and Related Research 150, 263–270.

Bradley, N., 2007. The response surface methodology. Department of Mathematical Sciences. South Bend, Indiana University. Master of Science in Applicaed Mathematics & Computer Science, 36–38.

Buti, F., Cacciagrano, D., Corradini, F., Merelli, E., Tesei, L., Pani, M., 2010. Bone remodelling in bioshape. Electronic Notes in Theoretical Computer Science 268, 17–29.

Carr, M.E., Carr, S.L., 1995. Fibrin structure and cocentration alter clot elastic-modulus but do not alter platelet-mediated force development. Blood Coagulation and Fibrinolysis 6 (1), 79–86.

Chen, C.C., Huang, T.H., Kao, C.T., Ding, S.J., 2006. Characterization of functionally graded hydroxyapatite/titanium composite coatings plasma-sprayed on Ti alloys. Journal of Biomedical Materials Research Part B-Applied Biomaterials 78B (1), 146–152.

Chen, Y., Zhou, S., Li, Q., 2009. Computational design for multifunctional microstructural composites. International Journal of Modern Physics B 23 (6-7), 1345–1351.

Chen, Y., Zhou, S., Li, Q., 2011. Microstructure design of biodegradable scaffold and its effect on tissue regeneration. Biomaterials 32 (22), 5003–5014.

Deporter, D.A., Watson, P.A., Pilliar, R.M., Chipman, M.L., Valiquette, N., 1990. A histological comparison in the dog of porous-coated vs threaded dental implants. J. Dent. Res. 69 (5), 1138–1145.

Dewidar, M.M., Lim, J.K., 2008. Properties of solid core and porous surface Ti-6Al-4V implants manufactured by powder metallurgy. Journal of Alloys and Compounds 454 (1–2), 442–446.

Esposito, M., Hirsch, J.M., Lekholm, U., Thomsen, P., 1998. Biological factors contributing to failures of osseointegrated oral implants (I). Success criteria and epidemiology. European Journal of Oral Sciences 106 (1), 527–551.

Feighan, J.E., Goldberg, V.M., Davy, D., Parr, J.A., Stevenson, S., 1995. The influence of surface-blasting on the incorporation of titanium-alloy implants in a rabbit intramedullary model. The Journal of Bone & Joint Surgery 77 (9), 1380–1395.

Field, C., Li, Q., Li, W., Thompson, M., Swain, M., 2010. Prediction of mandibular bone remodelling induced by fixed partial dentures. Journal of Biomechanics 43 (9), 1771–1779.

Field, C., Li, Q., Li, W., Thompson, M., Swain, M., 2012. A comparative mechanical and bone remodelling study of all-ceramic posterior inlay and onlay fixed partial dentures. Journal of Dentistry 40 (1), 48–56.

Fritsch, A., Hellmich, C., Dormieux, L., 2009. Ductile sliding between mineral crystals followed by rupture of collagen crosslinks: experimentally supported micromechanical explanation of bone strength. Journal of Theoretical Biology 260 (2), 230–252.

Frost, H.M., 2003. Bone's mechanostat: a 2003 update. The Anatomical Record Part A: Discoveries in Molecular, Cellular, and Evolutionary Biology 275A (2), 1081–1101.

Hou, S.J., Li, Q., Long, S.Y., Yanga, X.J., Li, W., 2008. Multiobjective optimization of multi-cell sections for the crashworthiness design. International Journal of Impact Engineering 35 (11), 1355–1367.

Itala, A.I., Ylanen, H.O., Ekholm, C., Karlsson, K.H., Aro, H.T., 2001. Pore diameter of more than 100 mu m is not requisite for bone ingrowth in rabbits. Journal of Biomedical Materials Research 58 (6), 679–683.

Keaveny, T.M., 2001. Strength of trabecular bone. In: Cowin, S.C. (Ed.), Bone Mechanics Handbook, 1. CRC Press LLC, Danvers, pp. 7.

Kim, S.J., Kim, M.R., Rim, J.S., Chung, S.M., Shin, S.W., 2010. Comparison of implant stability after different implant surface treatments in dog bone. Journal of Applied Oral Science 18 (4), 415–420.

Kunzler, T.P., Drobek, T., Schuler, M., Spencer, N.D., 2007. Systematic study of osteoblast and fibroblast response to roughness by means of surface-morphology gradients. Biomaterials 28 (13), 2175–2182.

Li, W., Swain, M.V., Li, Q., Steven, G.P., 2005. Towards automated 3D finite element modeling of direct fiber reinforced composite dental bridge. Journal of Biomedical Materials Research Part B: Applied Biomaterials 74B (1), 520–528.

Li, I., Li, H., Shi, L., Fok, A.S.L., Ucer, C., Deulin, H., Horner, K., Silikas, N., 2007. A mathematical model for simulating the bone remodeling process under mechanical stimulus. Dental Materials 23 (9), 1073–1078.

Li, W., Lin, D., Rungsiyakull, C., Zhou, S.W., Swain, M.V., Li, Q., 2011. Finite element based bone remodeling and resonance frequency analysis for osseointegration assessment of dental implant. Finite Elements in Analysis and Design 47, 898–905.

Lian, Z., Guan, H., Ivanovski, S., Loo, Y.C., Johnson, N.W., Zhang, H., 2010. Effect of bone to implant contact percentage on bone remodelling surrounding a dental implant. International Journal of Oral & Maxillofacial Surgery 39 (7), 690–698.

Lin, D., Li, Q., Li, W., Duckmanton, N., Swain, M., 2010a. Mandibular bone remodeling induced by dental implant. Journal of Biomechanics 43 (2), 287–293.

Lin, D., Li, Q., Li, W., Swain, M., 2009a. Dental implant induced bone remodeling and associated algorithms. Journal of the Mechanical Behavior of Biomedical Materials 2 (5), 410–432.

Lin, D., Li, Q., Li, W., Swain, M., 2010b. Bone remodeling induced by dental implants of functionally graded materials. Journal of Biomedical Materials Research Part B-Applied Biomaterials 92B (2), 430–438.

Lin, D., Li, Q., Li, W., Zhou, S.W., Swain, M.V., 2009b. Design optimization of functionally graded dental implant for bone remodeling. Composites Part B-Engineering 40 (7), 668–675.

Liu, X.Y., Niebur, G.L., 2008. Bone ingrowth into a porous coated implant predicted by a mechano-regulatory tissue differentiation algorithm. Biomechanics and Modeling in Mechanobiology 7 (4), 335–344.

Morra, M., Cassinelli, C., Cascardo, G., Cahalan, P., Cahalan, L., Fini, M., Giardino, R., 2003. Surface engineering of titanium by collagen immobilization. Surface characterization and in vitro and in vivo studies. Biomaterials 24 (25), 4639–4654.

Natali, A.N., Meroi, E.A., Williams, K.R., Calabrese, L., 1997. Investigation of the integration process of dental implants by means of a numerical analysis. Dental Materials 13 (5–6), 325–332.

Noble, B.S., Reeve, J., 2000. Osteocyte function, osteocyte death and bone fracture resistance. Molecular and Cellular Endocrinology 159 (1–2), 7–13.

O'Brien, W.J., 2008. Dental Materials and their Selection. Quintessence Publishing Co, Inc, Michigan.

Okazaki, K., Lee, W.H., Kim, D.K., Kopczyk, R.A., 1991. Physical characteristics of Ti-6Al-4V implants fabricated by electrodischarge compaction. Journal of Biomedical Materials Research 25 (12), 1417–1429.

Padhye, N., Branke, J., Mostaghim, S., Ieee, 2009. Empirical comparison of MOPSO methods—guide selection and diversity preservation. Ieee Congress on Evolutionary Computation, 1–5. Ieee, New York 2516–2523.

Podshivalov, L., Fischer, A., Bar-Yoseph, P.Z., 2011a. 3D hierarchical geometric modeling and multiscale FE analysis as a base for individualized medical diagnosis of bone structure. Bone 48 (4), 693–703.

Podshivalov, L., Fischer, A., Bar-Yoseph, P.Z., 2011b. Multiscale FE method for analysis of bone micro-structures. Journal of the Mechanical Behavior of Biomedical Materials 4 (6), 888–899.

Raquel, C.R., Naval, P.C., 2005. An effective use of crowding distance in multiobjective particle swarm optimization. In: Beyer, H.G. (Ed.), GECCO 2005: Genetic and Evolutionary Computation Conference, 1–2. Assoc Computing Machinery, New York, pp. 257–264.

Riha, P., Wang, X., Liao, R., Stoltz, J.F., 1999. Elasticity and fracture strain of whole blood clots. Clinical Hemorheological Microcirculation 21 (1), 45–49.

Romeed, S.A., Fok, S.L., Wilson, N.H.F., 2006. A comparison of 2D and 3D finite element analysis of a restored tooth. Journal of Oral Rehabilitation 33 (3), 209–215.

Rungsiyakull, C., Li, Q., Sun, G., Li, W., Swain, M.V., 2010. Surface morphology optimization for osseointegration of coated implants. Biomaterials 31 (27), 7196–7204.

Shen, H., Brinson, L.C., 2011. A numerical investigation of porous titanium as orthopedic implant material. Mechanics of Materials 43 (8), 420–430.

Shen, H., Li, H., Brinson, L.C., 2008. Effect of microstructural configurations on the mechanical responses of porous titanium: a numerical design of experiment analysis for orthopedic applications. Mechanics of Materials 40 (9), 708–720.

Sollazzo, V., Pezzetti, F., Scarano, A., Piattelli, A., Bignozzi, C.A., Massari, L., Brunelli, G., Carinci, F., 2008. Zirconium oxide coating improves implant osseointegration in vivo. Dental Materials 24 (3), 357–361.

Sturm, S., Zhou, S., Mai, Y.W., Li, Q., 2010. On stiffness of scaffolds for bone tissue engineering-a numerical study. Journal of Biomechanics 43 (9), 1738–1744.

Sun, G.Y., Li, G.Y., Zhou, S.W., Li, H.Z., Hou, S.J., Li, Q., 2011. Crashworthiness design of vehicle by using multiobjective robust optimization. Structural and Multidisciplinary Optimization 44 (1), 99–110.

Suzuki, K., Aoki, K., Ohya, K., 1997. Effects of surface roughness of titanium implants on bone remodeling activity of femur in rabbits. Bone 21 (6), 507–514.

Tanaka, E., Yamamoto, S., Nishida, T., Aoki, Y., 1999. A mathematical model of bone remodelling under overload and its application to evaluation of bone resportion around dental implants. Acta of Bioengineering and Biomechanics 1 (1), 117–121.

Tomaszewski, P.K., van Diest, M., Bulstra, S.K., Verdonschot, N., Verkerke, G.J., 2012. Numerical analysis of an osseointegrated prosthesis fixation with reduced bone failure risk and periprosthetic bone loss. Journal of Biomechanics 45 (11), 1875–1880.

Traini, T., Mangano, C., Sammons, R.L., Mangano, F., Macchi, A., Piattelli, A., 2008. Direct laser metal sintering as a new approach to fabrication of an isoelastic functionally graded material for manufacture of porous titanium dental implants. Dental Materials 24 (11), 1525–1533.

Vaillancourt, H., Pilliar, R.M., McCammond, D., 1995. Finite element analysis of crestal bone loss around porous-coated dental implants. Journal of Applied Biomaterials 6 (4), 267–282.

Wernig, F., Xu, Q., 2000. Mechanical stress-induced apoptosis in the cardiovascular system. Progress in Biophysics and Molecular Biology 78 (2–3), 105–137.

Xie, M., Yang, S.H., Win, H.L., Xiong, L.M., Huang, J.J., Zhou, J.G., 2010. Rabbit annulus fibrosus cell apoptosis induced by mechanical overload via a mitochondrial apoptotic pathway. Journal of Huazhong University of Science and Technology (Medical Sciences) 30 (3), 379–384.

Xue, W., Krishna, B.V., Bandyopadhyay, A., Bose, S., 2007. Processing and biocompatibility evaluation of laser processed porous titanium. Acta Biomaterials 3 (6), 1007–1018.

Yang, J., Xiang, H.-J., 2007. A three-dimensional finite element study on the biomechanical behavior of an FGBM dental implant in surrounding bone. Journal of Biomechanics 40 (11), 2377–2385.

Yang, Y.Z., Tian, J.M., Deng, L., Ong, J.L., 2002. Morphological behavior of osteoblast-like cells on surface-modified titanium in vitro. Biomaterials 23 (5), 1383–1389.

Yang, Y.Z., Tian, J.M., Tian, J.T., Chen, Z.Q., Deng, X.J., Zhang, D.H., 2000. Preparation of graded porous titanium coatings on titanium implant materials by plasma spraying. Journal of Biomedical Materials Research 52 (2), 333–337.